

# Multidimensional Triple Sum-Frequency Spectroscopy of MoS<sub>2</sub> and Comparisons with Absorption and Second Harmonic Generation Spectroscopies

Darien J. Morrow,<sup>1</sup> Daniel D. Kohler,<sup>1</sup> Kyle J. Czech,<sup>1</sup> and John C. Wright<sup>1, a)</sup>

*Department of Chemistry, University of Wisconsin–Madison, 1101 University Ave, Madison, WI 53706, United States*

(Dated: 9 July 2022)

Triple sum-frequency (TSF) spectroscopy is a recently-developed methodology that enables collection of multidimensional spectra by resonantly exciting multiple quantum coherences of molecular, vibrational, and electronic states. This work reports the first application of TSF to the electronic states of semiconductors. Two independently tunable ultrafast excitation pulses excite the A, B, and C features of a MoS<sub>2</sub> thin film. The TSF spectrum differs markedly from absorption and second harmonic generation spectra. The differences arise because of the relative importance of transition moments and the joint density of states. We develop a simple model and use global fitting of absorption and harmonic generation spectra to extract the joint density of states and the transition moments in these spectra. Our results validate previous assignments of the C feature to a large joint density of states created by band nesting.

Keywords: THG, TSF, CMDS, MoS<sub>2</sub>, TMDC

---

<sup>a)</sup>Electronic mail: [wright@chem.wisc.edu](mailto:wright@chem.wisc.edu)

Coherent multidimensional spectroscopy (CMDS) is a useful tool for exploring the rich many-body physics of semiconductors.<sup>1,2</sup> A new CMDS methodology is Triple Sum Frequency (TSF) spectroscopy. TSF is the non-degenerate analog of third harmonic generation (THG), and the four-wave mixing extension of three-wave mixing processes like sum-frequency generation and second harmonic generation (SHG).<sup>3</sup> TSF uses independently tunable ultrafast pulses to create coherences at increasingly higher frequencies while discriminating against transient populations. Scanning the multiple input pulse frequencies enables collection of a multidimensional spectrum. Cross peaks in the spectrum identify the dipole coupling between states. TSF has studied vibrational and electronic states of molecules.<sup>4-7</sup> This work reports the first TSF spectroscopy of a semiconductor.

We investigate a polycrystalline MoS<sub>2</sub> thin film. Transition metal dichalcogenides (TMDCs), such as MoS<sub>2</sub>, are layered semiconductors whose indirect bandgaps become direct in the monolayer limit.<sup>8,9</sup> TMDCs exhibit strong spin-orbit coupling, high charge mobility, and have novel photonic capabilities.<sup>10-12</sup> The optical spectrum of MoS<sub>2</sub> is dominated by three features: A ( $\hbar\omega \approx 1.8$  eV), B ( $\hbar\omega \approx 1.95$  eV), and C ( $\hbar\omega \approx 2.7$  eV).<sup>13,14</sup> A and B originate from high binding energy excitonic transitions between spin-orbit split bands.<sup>13,15-18</sup> The stronger C feature is predicted to arise from a large joint density of states (JDOS) due to band nesting across a large section of the Brillouin zone (BZ).<sup>19-22</sup> As of yet, no direct, experimental verification of the large JDOS defining the C feature has been accomplished. In this work, we demonstrate how first, second, and third order spectroscopies can be used together to determine whether the prominence of a feature is due to its transition dipole or a transition degeneracy.

The spectroscopies considered here can be understood in the electric dipole approximation using perturbation theory.<sup>23,24</sup> Briefly, an electric field ( $E$ ) drives a polarization ( $P$ ) in the material. The polarization is related to an oscillating coherence between two states. The polarization is expressed as an expansion in electric field and susceptibility ( $\chi$ ) order. Absorption, SHG, and TSF (THG) depend on  $\chi^{(1)}$ ,  $\chi^{(2)}$ , and  $\chi^{(3)}$ , respectively. As is well known, SHG response requires broken inversion symmetry while first and third order responses do not; SHG is sensitive only to the interfaces of the MoS<sub>2</sub>, while the other spectroscopies interrogate the entire film. In the limit of very thin films (no interference or velocity-mismatch effects), the measured electric field intensity observed in SHG and TSF is proportional to  $|\chi^{(2)}|^2$  and  $|\chi^{(3)}|^2$ , respectively. All of the discussed spectroscopies rely

on resonant enhancement to detect state coupling. When a driving laser is resonant with an interstate transition,  $\chi$  is large and causes an increase in output intensity. We look for cross-peaks between multiple, scanned driving lasers in order to observe dipole coupling between states.<sup>4-6</sup> Our TSF work adds a multidimensional component to the extensive SHG and THG spectroscopy and microscopy work on TMDCs already accomplished by many workers.<sup>25-38</sup>

Nonlinear measurements of thin films are often complicated by non-resonant substrate contributions which are mitigated by measuring the coherent output in the reflected instead of transmitted direction.<sup>39-43</sup> We prepared a 10 nm thick MoS<sub>2</sub> thin film by first evaporating Mo onto the fused silica substrate followed by sulfidation of the Mo.<sup>40,44</sup> Our sample substrate is a fused silica prism so that back-reflected, non-resonant TSF exits the substrate traveling parallel to the desired TSF signal but shifted spatially. Synthesis details, AFM measurements to determine film thickness, and a Raman spectrum are present in the SI.

For our TSF measurements, an ultrafast oscillator seeds a regenerative amplifier, creating pulses centered at 1.55 eV with a 1 kHz repetition rate. These pulses pump two optical parametric amplifiers (OPAs) which create tunable pulses of light from  $\sim 0.5$  to  $\sim 1$  eV with spectral width on the amplitude level of FWHM  $\approx 46$  meV. The two beams with frequencies  $\omega_1$  &  $\omega_2$  and wave vectors  $\vec{k}_1$  &  $\vec{k}_2$  are focused onto the sample. All beams are linearly polarized (S relative to sample) and coincident in time. The spatially coherent output with wave vector  $-\left(\vec{k}_1 + 2\vec{k}_2\right)$  is isolated with an aperture (the negative signs correspond to the reflective direction), focused into a monochromator, and detected with a photomultiplier tube. The TSF intensity is linear in  $\omega_1$  fluence and quadratic in  $\omega_2$  fluence (see the SI for details). The SI contains additional experimental and calibration details. All raw data, workup scripts, and simulation scripts used in the creation of this work are permissively licensed and publicly available for reuse.<sup>45</sup> Our acquisition,<sup>46</sup> workup,<sup>47</sup> and modeling software<sup>45</sup> are built on top of the open source, publicly available Scientific Python ecosystem.<sup>48-50</sup>

Our main experimental result is a 2D TSF spectrum of a MoS<sub>2</sub> thin film (Figure 1) acquired with a tracking monochromator at frequency  $\omega_m = \omega_\Sigma \equiv \omega_1 + 2\omega_2$ . The measured MoS<sub>2</sub> TSF spectrum is normalized by the measured TSF spectrum of the fused silica substrate in order to account for spectrally-dependent OPA output intensities and detector responsivity. The TSF spectrum of MoS<sub>2</sub> is relatively featureless with all features running

parallel to a line with slope of  $-1/2$ . A slope of  $-1/2$  implies that the output frequency,  $\omega_\Sigma$ , largely determines the resonant enhancement. Peaks at output colors  $\sim 1.85$  &  $\sim 2.0$  eV and a broad trough at output color  $\sim 2.56$  eV are present in Figure 1. The inset of Figure 1 diagrams the cases where either the last interaction (left) is resonant or the second to last interaction is resonant (right). We exclusively observe the former case. The lack of “two-photon resonances” when  $2\omega_2$  traces over the A and B feature energies was surprising to us given the large two-photon absorption cross-section of  $\text{MoS}_2$ .<sup>51</sup> The two-photon resonances would manifest as horizontal features in Figure 1. Coupling between A and C (or B and C) would manifest as a cross-hatch of features in the TSF spectrum. For instance, if A and C were coupled we would see a horizontal feature at  $\hbar\omega_2 = \hbar\omega_A/2 \approx 0.9$  eV interacting with a vertical feature at  $\hbar\omega_1 = \hbar(\omega_C - \omega_A) \approx 0.9$  eV. We do not observe these peaks, and therefore do not observe inter-feature, coherent, optical coupling.

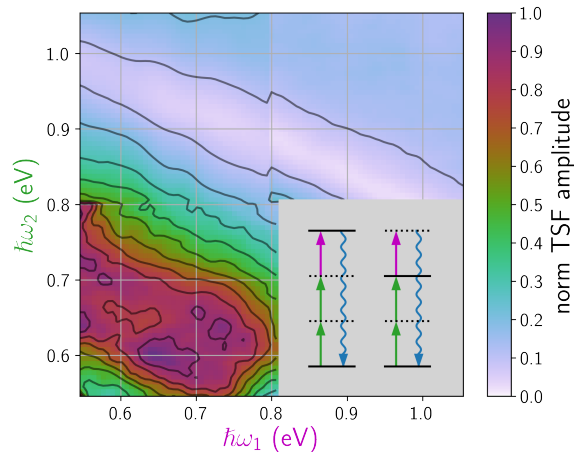


FIG. 1. Normalized 2D TSF spectra of  $\text{MoS}_2$ . Inset diagrams processes where the third interaction is resonant with a state (left) and when the second interaction is resonant with a state (right). The measured output is represented by a wavy downward arrow. Note, the gray area of the inset was not experimentally explored.

Since the dominant spectral features in Figure 1 depend only on output color, we can generate a 1D THG spectrum by plotting the mean TSF amplitude for each output color. The THG spectrum is compared with other techniques in Figure 2. Due to the unconventional prism substrate, we were unable to acquire an absorption spectrum of the sample, but we

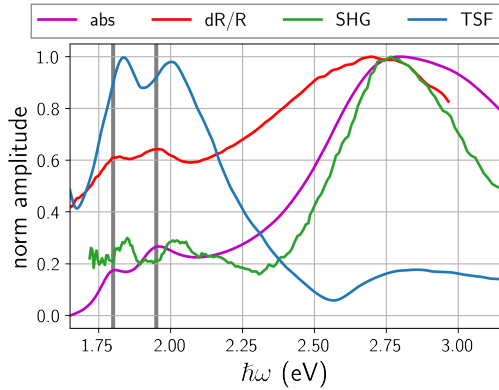


FIG. 2. Normalized amplitude 1D spectra of MoS<sub>2</sub> thin films: absorption<sup>40</sup>, SHG<sup>32</sup>, reflection contrast (dR/R), and TSF (THG). The TSF spectrum is derived from Figure 1 as detailed in the main text. Vertical gray bars are guides to the eye set at 1.80 and 1.95 eV to demonstrate how SHG and TSF features are blue shifted from absorption and dR/R spectral peaks.

did acquire a reflection contrast spectrum shown in Figure 2.<sup>52,53</sup> The absorption spectrum presented in Czech *et al.*<sup>40</sup> and Figure 2 is of a sample prepared with similar conditions as our sample, but on a flat substrate. The A and B feature peaks of the THG spectrum are blue-shifted compared to the absorption spectrum. Wang *et al.*<sup>28</sup> observed a similar blue shift when they measured the THG spectrum of MoS<sub>2</sub> around the A and B features. The C feature is dominant in the SHG<sup>32</sup> and absorption spectrum<sup>40</sup> while the A and B features are dominant in the THG spectrum. This observation is the main motivation for our analysis.

To explain why C dominates the absorption and SHG spectra but not the THG spectrum, we develop a simple model. To our knowledge, a unified model for comparing large dynamic-range absorption, SHG, and THG spectra of a semiconductor does not exist. Notable headway has been made to calculate SHG spectra<sup>54</sup> and write closed equations of motion<sup>55</sup> for semiconductors, but simple formalisms are lacking. The lack of formalisms is especially glaring when trying to compare large dipole excitonic transitions with large JDOS interband transitions because many authors write the dipole as a constant with respect to both transition energy and band momentum. We develop our simple model by expanding the typical linear response formalism for direct transitions of semiconductors to include sum-frequency processes.

In the case of  $\chi^{(1)}$ , simple theories exist for expanding the single oscillator case to bulk conditions. For more than one oscillator, the total susceptibility is the sum of individual susceptibilities. For a semiconductor system, this is a summation over all wave-vectors,  $\{\mathbf{k}\}$  such that  $\mathbf{k} \in \text{BZ}$ :

$$\chi^{(1)}(-\omega_1, \omega_1) = \sum_{a,g} \sum_{\mathbf{k}} \frac{\mu_{g\mathbf{a}\mathbf{k}}^2}{\Delta_{g\mathbf{a}\mathbf{k}}^1}, \quad (1)$$

where  $\Delta_{g\mathbf{a}\mathbf{k}}^1 = \omega_{g\mathbf{a}\mathbf{k}} - \omega_1 - i\Gamma$  and  $\Gamma$  is a damping rate which accounts for the finite width of the optical transitions. It is common to replace the summation with a transition energy distribution function between conduction band  $x$  and valence band  $y$ ,  $J_{xy}(E)$ ,<sup>56</sup> such that

$$\chi^{(1)}(-\omega_1, \omega_1) \propto \int \frac{dE}{E - \hbar\omega_1 - i\hbar\Gamma} \sum_{x,y} J_{xy}(E) \mu_{xy}(E)^2. \quad (2)$$

In crystals,  $J_{xy}(E)$  is the JDOS. Note the dependence of the susceptibility on both  $J_{xy}(E)$  and  $\mu_{xy}(E)^2$ . In the case that either the JDOS or the transition dipole are constant, spectroscopy techniques can be used to locate excitonic transitions or critical points in the JDOS. If the JDOS and transition dipole both vary, then traditional techniques fail.

The THG and SHG responses take the form of:

$$\chi^{(2)}(-\omega_{21}, \omega_1, \omega_2) = \mathcal{P} \sum_{b,a,g} \sum_{\mathbf{k}} \frac{\mu_{g\mathbf{b}\mathbf{k}} \mu_{b\mathbf{a}\mathbf{k}} \mu_{a\mathbf{g}\mathbf{k}}}{\Delta_{g\mathbf{b}\mathbf{k}}^{12} \Delta_{g\mathbf{a}\mathbf{k}}^1} \quad (3)$$

$$\chi^{(3)}(-\omega_{321}, \omega_1, \omega_2, \omega_3) = \mathcal{P} \sum_{c,b,a,g} \sum_{\mathbf{k}} \frac{\mu_{g\mathbf{c}\mathbf{k}} \mu_{c\mathbf{b}\mathbf{k}} \mu_{b\mathbf{a}\mathbf{k}} \mu_{a\mathbf{g}\mathbf{k}}}{\Delta_{g\mathbf{c}\mathbf{k}}^{123} \Delta_{g\mathbf{b}\mathbf{k}}^{12} \Delta_{g\mathbf{a}\mathbf{k}}^1}, \quad (4)$$

where  $c, b, a$ , and  $g$  are bands of the semiconductor. We have defined  $\omega_{21} \equiv \omega_2 + \omega_1$  and  $\omega_{321} \equiv \omega_3 + \omega_2 + \omega_1$ .  $\mathcal{P}$  is a permutation operator which accounts for all combinations of field-matter interactions. The additional detuning factors are defined by  $\Delta_{g\mathbf{c}\mathbf{k}}^{123} \equiv \omega_{c\mathbf{g}\mathbf{k}} - \omega_{321} - i\Gamma$  and  $\Delta_{g\mathbf{b}\mathbf{k}}^{12} \equiv \omega_{b\mathbf{g}\mathbf{k}} - \omega_{21} - i\Gamma$  in which  $\omega_{ab}$  is the frequency difference between bands  $a$  and  $b$  at point  $\mathbf{k}$  in the BZ. The JDOS formalism employed in Equation 2 can be abstracted to describe  $\chi^{(2)}$  and  $\chi^{(3)}$  with the introduction of multidimensional joint density functions. These joint densities depend not just on the energy difference between the initial and final states, but also on the energy differences between the intermediate states reached during the sum-frequency process. See the SI for further details.

To simulate the spectra, the sum over bands in Equation 2-Equation 4 is truncated at three total bands: the valence band,  $v$ , the conduction band,  $c$ , and a third higher-energy

band,  $b$ . The SHG and THG spectra are measured close to the direct bandgap, so transitions between  $c$  and  $v$  are key to describing the response. The  $b$  band is taken to be a much higher energy (6 eV) than the valence band. We define the transition strength of low-lying states ( $c$  and  $v$ ) to this nondescript high-lying band with the parameter  $\mu_{\text{NR}}(\hbar\omega)$ . We note that  $\mu_{\text{NR}}$  is not formally a dipole, but instead collects together all non-resonant transition factors involving band  $b$  (dipoles and degeneracies between  $c$  and  $b$  or  $v$  and  $b$ ). While this is an improper parameterization of the actual band structure above the conduction band and below the valence band, its inclusion is crucial for reproducing details of our spectra, and the parameters offer insight into the role of virtual states in sum-frequency spectroscopies.

With this framework, we can now reason why THG, SHG, and absorption measurements are complementary for distinguishing degeneracy and dipole moments. The strength of absorption is proportional to  $\mu_{cv}^2$  and  $J_{cv}$  (Equation 2). SHG signals will be due to the sequence  $v \rightarrow b \rightarrow c$ , which informs on the non-resonant band  $b$ . THG has sequences such as  $v \rightarrow c \rightarrow v \rightarrow c$ , which scale as  $\mu_{cv}^4$  but are still linear in  $J_{cv}$ . On the other hand, THG can depend on state  $b$  and consequently depends on the same non-resonant features of SHG. THG and absorption give different scalings for transitions between  $c$  and  $v$ , but SHG is also needed to constrain the non-resonant transitions of THG involving band  $b$ .

Figure 3 summarizes the fit of our model to experiment. Our simulation uses a discrete set of transition energies to approximate the integral of Equation 2. We employ 140 discrete energies spaced 20 meV apart with  $\Gamma = 20$  meV,  $\hbar\omega_{b_j} = 6$  eV, and  $\Gamma_b = 500$  meV. Our strategy of a discretized set of transition energies is similar to the constrained variational analysis that is often employed to relate a material's reflection spectrum to its absorption or dielectric spectra.<sup>14,57,58</sup> The model extracts the dipole strength of the  $c \leftrightarrow v$  transitions,  $\mu_{cv}$ , as well as a weighting factor for transitions involving the non-resonant state,  $\mu_{\text{NR}}$ . See the SI for further modeling details; note some intrinsic uncertainty is present in our model because we compare measurements accomplished on thin film MoS<sub>2</sub> samples with differing layer number.

Figure 3a shows qualitative agreement between the model and experiment. Our model is agnostic to the functional form of the JDOS or dipole spectra, so we can compare the response from an excitonic transition to that of an interband transition. The fitted parameters are shown in Figure 3b and Figure 3c; note how  $\mu_{cv}$  and  $\mu_{\text{NR}}$  both demonstrate peaked features in the A and B feature region where  $J_{cv}$  is minimized. As  $\hbar\omega$  increases from

the B feature,  $J_{cv}$  drastically increases while  $\mu_{cv}$  and  $\mu_{NR}$  both decrease—the increase in  $J_{cv}$  is analogous to the large JDOS attributed to band nesting by recent workers.<sup>19–21</sup> For comparison, in Figure 3c we plot the JDOS as recently calculated by Bieniek *et al.*<sup>22</sup> for monolayer MoS<sub>2</sub> within their tight-binding model. Observe how both the simulated JDOS and the tight-binding, monolayer JDOS have a small value near the A and B features but form a peaked structure near the C feature. Our fitting procedure convincingly reproduces the large degeneracy of the C feature due to band-nesting. To the red of the A feature, the JDOS and  $\mu_{NR}$  increase while  $\mu_{cv}$  decays to zero. We attribute this behavior to an artifact of our finite spectral bandwidth. In the first-order case, our fitting method is known to have difficulty with the edges of spectra.<sup>59</sup>

Using the fit parameters, we also calculate a 2D TSF spectrum as shown in Figure 3d. Much like Figure 1, the dominant TSF features predicted by our model are parallel to a line of constant output color. A small dip is seen in our model over the line  $\hbar(\omega_1 + \omega_2) = 1.7$  eV. Above this line, there are some resonances which are from sequences like  $v \rightarrow b \rightarrow c \rightarrow b$  in which resonant enhancement comes from the second interaction. Below the line, the dominant features come from coherence pathways like  $v \rightarrow c \rightarrow b \rightarrow c$  or  $v \rightarrow c \rightarrow v \rightarrow c$ , in which the third excitation is resonant. Our model fails to capture some features of the three optical measurements. For instance, the model fails to capture the deep trough seen in Figure 1, shifts the position of A and B absorption features, and undershoots the THG spectrum at energies above 2.7 eV.

In summary, our TSF measurements uncover a conspicuous difference between absorption, SHG, and TSF spectra: the C feature is prominent in absorption and SHG but not TSF. We address this conundrum by extracting the spectrally dependent dipole and JDOS using all three spectra. We find the differences in the spectra arise because the C feature has a large JDOS and small dipole compared to the A and B features. We hope our measurements and analysis catalyze a renewed interest in elucidating the full spectral features of semiconductors by combining the results of many orders of complementary spectroscopies. Our measurements demonstrate the utility of non-linear, sum-frequency spectroscopies of semiconductor nanostructures over a wide range of excitation frequencies. In the future, our work can be extended to examine the coupling of multiple transitions which originate at the same point in the BZ and thus elucidate how different conduction or valence bands interact with each other.

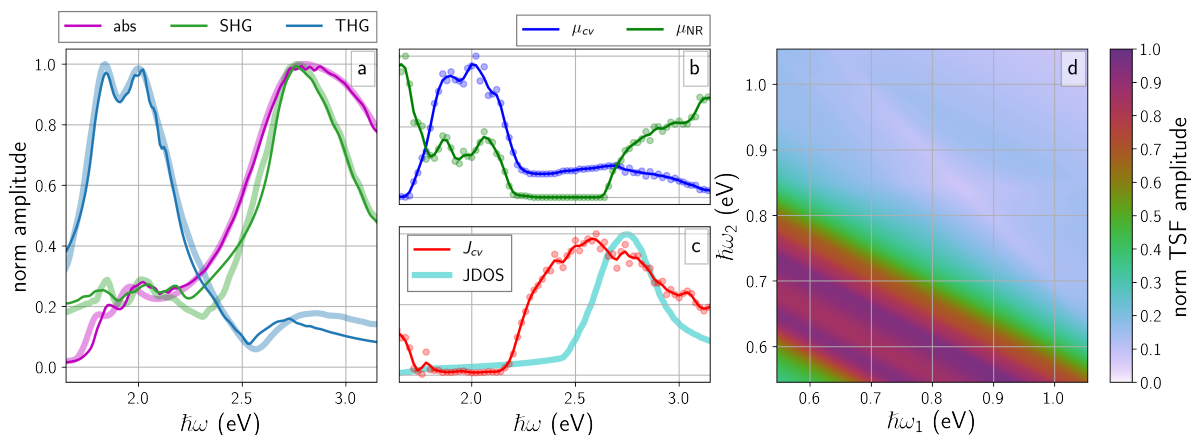


FIG. 3. Variational model of optical spectroscopies. (a) normalized comparison of experiment (thick, translucent lines, absorption<sup>40</sup> and SHG<sup>32</sup>) and model (thin lines). (b) normalized model dipole parameters in experimentally explored range. (c) normalized model density,  $J_{cv}$ , and tight-binding optical JDOS from Bieniek *et al.*<sup>22</sup>. (d) normalized TSF spectrum as predicted by our model as fit to 1D experiments.

## SUPPLEMENTARY INFORMATION

See Supplemental Information for synthesis and characterization of our MoS<sub>2</sub> thin film, more discussion of our ultrafast instrument and its calibration, discussion of data normalization scheme, discussion of our model, and additional simulation details

## ACKNOWLEDGMENTS

This work was supported by the Department of Energy, Office of Basic Energy Sciences, Division of Materials Sciences and Engineering, under award DE-FG02-09ER46664. The authors thank K. Lloyd for performing AFM measurements and T. Pedersen for sharing the SHG data used in this work.

## REFERENCES

- <sup>1</sup>S. T. Cundiff, *Optics Express* **16**, 4639 (2008).
- <sup>2</sup>G. Moody and S. T. Cundiff, *Optics Express* **2**, 641 (2017).

- <sup>3</sup>N. A. Neff-Mallon and J. C. Wright, *Analytical Chemistry* **89**, 13182 (2017).
- <sup>4</sup>E. S. Boyle, A. V. Pakoulev, and J. C. Wright, *The Journal of Physical Chemistry A* **117**, 5578 (2013).
- <sup>5</sup>E. S. Boyle, N. A. Neff-Mallon, and J. C. Wright, *The Journal of Physical Chemistry A* **117**, 12401 (2013).
- <sup>6</sup>E. S. Boyle, N. A. Neff-Mallon, J. D. Handali, and J. C. Wright, *The Journal of Physical Chemistry A* **118**, 3112 (2014).
- <sup>7</sup>M. Grechko, T. Hasegawa, F. D'Angelo, H. Ito, D. Turchinovich, Y. Nagata, and M. Bonn, *Nature Communications* **9** (2018), 10.1038/s41467-018-03303-y.
- <sup>8</sup>K. F. Mak, C. Lee, J. Hone, J. Shan, and T. F. Heinz, *Physical Review Letters* **105** (2010), 10.1103/physrevlett.105.136805.
- <sup>9</sup>J. K. Ellis, M. J. Lucero, and G. E. Scuseria, *Applied Physics Letters* **99**, 261908 (2011).
- <sup>10</sup>Q. H. Wang, K. Kalantar-Zadeh, A. Kis, J. N. Coleman, and M. S. Strano, *Nature Nanotechnology* **7**, 699 (2012).
- <sup>11</sup>F. Xia, H. Wang, D. Xiao, M. Dubey, and A. Ramasubramaniam, *Nature Photonics* **8**, 899 (2014).
- <sup>12</sup>K. F. Mak and J. Shan, *Nature Photonics* **10**, 216 (2016).
- <sup>13</sup>A. Molina-Sánchez, D. Sangalli, K. Hummer, A. Marini, and L. Wirtz, *Physical Review B* **88** (2013), 10.1103/physrevb.88.045412.
- <sup>14</sup>Y. Li, A. Chernikov, X. Zhang, A. Rigosi, H. M. Hill, A. M. van der Zande, D. A. Chenet, E.-M. Shih, J. Hone, and T. F. Heinz, *Physical Review B* **90** (2014), 10.1103/physrevb.90.205422.
- <sup>15</sup>D. Y. Qiu, F. H. da Jornada, and S. G. Louie, *Physical Review Letters* **111** (2013), 10.1103/physrevlett.111.216805.
- <sup>16</sup>K. He, N. Kumar, L. Zhao, Z. Wang, K. F. Mak, H. Zhao, and J. Shan, *Physical Review Letters* **113** (2014), 10.1103/physrevlett.113.026803.
- <sup>17</sup>N. Saigal, V. Sugunakar, and S. Ghosh, *Applied Physics Letters* **108**, 132105 (2016).
- <sup>18</sup>J. Kopaczek, M. P. Polak, P. Scharoch, K. Wu, B. Chen, S. Tongay, and R. Kudrawiec, *Journal of Applied Physics* **119**, 235705 (2016).
- <sup>19</sup>L. Britnell, R. M. Ribeiro, A. Eckmann, R. Jalil, B. D. Belle, A. Mishchenko, Y.-J. Kim, R. V. Gorbachev, T. Georgiou, S. V. Morozov, A. N. Grigorenko, A. K. Geim, C. Casiraghi, A. H. C. Neto, and K. S. Novoselov, *Science* **340**, 1311 (2013).

- <sup>20</sup>A. Carvalho, R. M. Ribeiro, and A. H. C. Neto, *Physical Review B* **88** (2013), [10.1103/physrevb.88.115205](#).
- <sup>21</sup>J. Jeong, Y.-H. Choi, K. Jeong, H. Park, D. Kim, and M.-H. Cho, *Physical Review B* **97** (2018), [10.1103/physrevb.97.075433](#).
- <sup>22</sup>M. Bieniek, M. Korkusiński, L. Szulakowska, P. Potasz, I. Ozfidan, and P. Hawrylak, *Physical Review B* **97** (2018), [10.1103/physrevb.97.085153](#).
- <sup>23</sup>R. W. Boyd, *Nonlinear Optics*, 3rd ed. (Academic Press, 2008).
- <sup>24</sup>N. Bloembergen and Y. R. Shen, *Physical Review* **133**, A37 (1964).
- <sup>25</sup>Y. Li, Y. Rao, K. F. Mak, Y. You, S. Wang, C. R. Dean, and T. F. Heinz, *Nano Letters* **13**, 3329 (2013).
- <sup>26</sup>L. M. Malard, T. V. Alencar, A. P. M. Barboza, K. F. Mak, and A. M. de Paula, *Physical Review B* **87** (2013), [10.1103/physrevb.87.201401](#).
- <sup>27</sup>N. Kumar, S. Najmaei, Q. Cui, F. Ceballos, P. M. Ajayan, J. Lou, and H. Zhao, *Physical Review B* **87** (2013), [10.1103/physrevb.87.161403](#).
- <sup>28</sup>R. Wang, H.-C. Chien, J. Kumar, N. Kumar, H.-Y. Chiu, and H. Zhao, *ACS Applied Materials & Interfaces* **6**, 314 (2013).
- <sup>29</sup>M. L. Trolle, G. Seifert, and T. G. Pedersen, *Physical Review B* **89** (2014), [10.1103/physrevb.89.235410](#).
- <sup>30</sup>M. Grüning and C. Attaccalite, *Physical Review B* **89** (2014), [10.1103/physrevb.89.081102](#).
- <sup>31</sup>D. J. Clark, V. Senthilkumar, C. T. Le, D. L. Weerawarne, B. Shim, J. I. Jang, J. H. Shim, J. Cho, Y. Sim, M.-J. Seong, S. H. Rhim, A. J. Freeman, K.-H. Chung, and Y. S. Kim, *Physical Review B* **90** (2014), [10.1103/physrevb.90.121409](#).
- <sup>32</sup>M. L. Trolle, Y.-C. Tsao, K. Pedersen, and T. G. Pedersen, *Physical Review B* **92** (2015), [10.1103/physrevb.92.161409](#).
- <sup>33</sup>G. Wang, X. Marie, I. Gerber, T. Amand, D. Lagarde, L. Bouet, M. Vidal, A. Balocchi, and B. Urbaszek, *Physical Review Letters* **114** (2015), [10.1103/physrevlett.114.097403](#).
- <sup>34</sup>J. Sun, Y.-J. Gu, D. Y. Lei, S. P. Lau, W.-T. Wong, K.-Y. Wong, and H. L.-W. Chan, *ACS Photonics* **3**, 2434 (2016).
- <sup>35</sup>L. Karvonen, A. Säynätjoki, M. J. Huttunen, A. Autere, B. Amirsolaimani, S. Li, R. A. Norwood, N. Peyghambarian, H. Lipsanen, G. Eda, K. Kieu, and Z. Sun, *Nature Communications* **8**, 15714 (2017).

- <sup>36</sup>M. J. Shearer, L. Samad, Y. Zhang, Y. Zhao, A. Purotzky, K. W. Eliceiri, J. C. Wright, R. J. Hamers, and S. Jin, [Journal of the American Chemical Society](#) **139**, 3496 (2017).
- <sup>37</sup>M. M. Glazov, L. E. Golub, G. Wang, X. Marie, T. Amand, and B. Urbaszek, [Physical Review B](#) **95** (2017), [10.1103/physrevb.95.035311](#).
- <sup>38</sup>N. K. Balla, M. O'Brien, N. McEvoy, G. S. Duesberg, H. Rigneault, S. Brasselet, and D. McCloskey, [ACS Photonics](#) (2018), [10.1021/acsp Photonics.7b00912](#).
- <sup>39</sup>A. Volkmer, J.-X. Cheng, and X. S. Xie, [Physical Review Letters](#) **87** (2001), [10.1103/physrevlett.87.023901](#).
- <sup>40</sup>K. J. Czech, B. J. Thompson, S. Kain, Q. Ding, M. J. Shearer, R. J. Hamers, S. Jin, and J. C. Wright, [ACS Nano](#) **9**, 12146 (2015).
- <sup>41</sup>D. J. Morrow, D. D. Kohler, and J. C. Wright, [Physical Review A](#) **96** (2017), [10.1103/physreva.96.063835](#).
- <sup>42</sup>J. D. Handali, K. F. Sunden, E. M. Kaufman, and J. C. Wright, [Chemical Physics](#) (2018), [10.1016/j.chemphys.2018.05.023](#).
- <sup>43</sup>A. Honold, L. Schultheis, J. Kuhl, and C. W. Tu, [Applied Physics Letters](#) **52**, 2105 (1988).
- <sup>44</sup>M. R. Laskar, L. Ma, S. Kannappan, P. S. Park, S. Krishnamoorthy, D. N. Nath, W. Lu, Y. Wu, and S. Rajan, [Applied Physics Letters](#) **102**, 252108 (2013).
- <sup>45</sup>D. Morrow, D. Kohler, K. Czech, and J. Wright, (2018), [10.17605/osf.io/2wff6g](#).
- <sup>46</sup>B. J. Thompson, K. F. Sunden, D. J. Morrow, and N. A. Neff-Mallon, "PyCMDS," (2018).
- <sup>47</sup>B. J. Thompson, K. F. Sunden, D. J. Morrow, N. A. Neff-Mallon, K. J. Czech, D. D. Kohler, and R. Swedin, "WrightTools," (2018).
- <sup>48</sup>E. Jones, T. Oliphant, and P. Peterson, "SciPy: Open source scientific tools for Python," (2001), [Online; accessed 2017-09-28].
- <sup>49</sup>S. van der Walt, S. C. Colbert, and G. Varoquaux, [Computing in Science & Engineering](#) **13**, 22 (2011).
- <sup>50</sup>J. D. Hunter, [Computing in Science & Engineering](#) **9**, 90 (2007).
- <sup>51</sup>S. Zhang, N. Dong, N. McEvoy, M. O'Brien, S. Winters, N. C. Berner, C. Yim, Y. Li, X. Zhang, Z. Chen, L. Zhang, G. S. Duesberg, and J. Wang, [ACS Nano](#) **9**, 7142 (2015).
- <sup>52</sup>J. McIntyre and D. Aspnes, [Surface Science](#) **24**, 417 (1971).
- <sup>53</sup>K. F. Mak, M. Y. Sfeir, Y. Wu, C. H. Lui, J. A. Misewich, and T. F. Heinz, [Physical Review Letters](#) **101** (2008), [10.1103/physrevlett.101.196405](#).

- <sup>54</sup>J. E. Sipe and A. I. Shkrebtii, [Physical Review B \*\*61\*\*, 5337 \(2000\)](#).
- <sup>55</sup>V. M. Axt and S. Mukamel, [Reviews of Modern Physics \*\*70\*\*, 145 \(1998\)](#).
- <sup>56</sup>Equation 1, and all further theory developed, neglect indirect transitions. We find this a reasonable assumption since our multidimensional spectrum exhibited no cross-peaks between the K-point features (A and B) and the C band.
- <sup>57</sup>A. B. Kuzmenko, [Review of Scientific Instruments \*\*76\*\*, 083108 \(2005\)](#).
- <sup>58</sup>E. J. Sie, A. J. Frenzel, Y.-H. Lee, J. Kong, and N. Gedik, [Physical Review B \*\*92\*\* \(2015\), 10.1103/physrevb.92.125417](#).
- <sup>59</sup>D. M. Roessler, [British Journal of Applied Physics \*\*16\*\*, 1119 \(1965\)](#).